Photochemistry of bismuth- and silver-containing glasses under femtosecond laser irradiation: energy transfers and 3D-localized background-free near-infrared fluorescence emission

Fouad Alassani, Nadège Ollier, Guillaume Raffy, Alexandre Fargues, André del Guerzo, Lionel Canioni, Thierry Cardinal, Yannick Petit

Photochemistry of Bismuth and Silver Containing Glasses under Femtosecond Laser Irradiation: Energy Transfers and 3D-localized Background-Free Near-Infrared Fluorescence Emission

Fouad Alassani[1,2], Nadège Ollier[2], Guillaume Raffy[3], Alexandre Fargues[1], André Del Guerzo[3], Lionel Canioni[1], Thierry Cardinal[1], Yannick Petit[1,*]

1 *Université de Bordeaux, CNRS, Bordeaux INP, ICMCB, UMR 5026, F-33600 Pessac, France*
2 *Laboratoire des Solides Irradiés, UMR 7642 CEA-CNRS-Ecole Polytechnique, Palaiseau, France*
3 *Université de Bordeaux, CNRS, Institute of Molecular Sciences (ISM, UMR 5255), F-33400 Talence, France*

Corresponding author: yannick.petit@u-bordeaux.fr

Abstract

Tunable fluorescence property from visible to near-infrared (NIR) of high-localized 3D architecture down to the diffraction limit thanks to femtosecond (fs) Direct Laser Writing (DLW) in Bismuth-doped silver-containing glass is performed. Absorption and photo-luminescent spectroscopy showed evidence of the homogenous dispersion of bismuth ions (Bi^{3+}) and silver ions in the glass matrix before DLW. High repetition rate fs DLW inducing simultaneously the photochemistry of silver ions and the photo-redox reaction of bismuth ions has been obtained. Fs DLW allows the creation of 3D fluorescence patterns formed by co-localization of silver cluster and low valence bismuth ions exhibiting an emission band covering the whole visible to the NIR wave range. The phenomena of electron transfer from silver atoms to bismuth ions and the non-radiative energy transfer from silver clusters to NIR emitting bismuth ions are demonstrated.

Keywords: Femtosecond, Photochemistry, Photo-reduction, Silver clusters, Bismuth, Energy transfer, 3D structures.

TOC Graphic

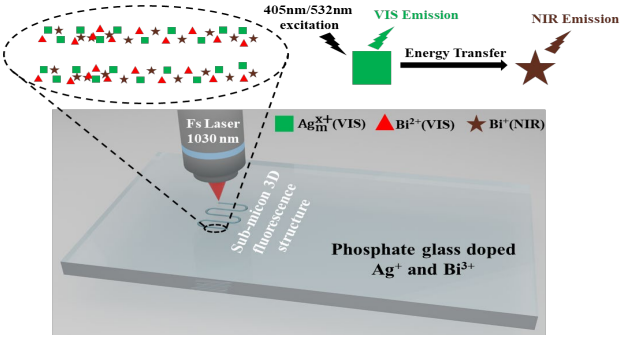

1. Introduction

Still in the scope to push scientific discovery over its actual limit, many efforts in recent years have been made at the interface of physics and chemistry to go further down to the diffraction limit to design new

photonic components in transparent dielectrics. Miniaturization of 3D multiscale architecture is indeed of interest for the development of Photonic Integrated Circuit (PIC) and applications in several areas such as sensing, data communication, biomedical and optical storage[1–5]. The unique advantage of Femtosecond (fs) Direct Laser Writing (DLW) due to its flexibility, ultrafast micro processing, and high precision allows high-localized modification of photosensitive transparent dielectric resulting to low scale photonic component (PIC). Recently, we have demonstrated the capability to structure the local fluorescence property of silver-containing glasses using fs DLW allowing the local creation of an elementary brick with inner features down the diffraction limit (<100 nm)[6–9]. This structuration relies on the creation of highly fluorescent silver clusters (Ag_m^{x+}) formed by local aggregation of silver atoms (Ag^0) and silver ions (Ag^+) thanks to fs laser-activated redox reactivity and migration of silver ions in the glass matrix[10]. For UV to Visible excitation, such a laser-induced silver cluster-containing structure exhibits a broad emission band in the visible. To extend the emission spectrum from the visible to the red and NIR(infrared), the possibility to create an interaction between silver and other fluorescent ions such as noble metal or Rare Earth ions in glass bulk was reported thanks to resonant energy transfer or local field effect phenomena[11–13]. However, monitoring highly localized 3D structures of tunable localized fluorescence in glass remains a challenge. We have recently demonstrated the laser-induced highly localized 3D structure with high contrast and tunable fluorescence property in the whole visible and NIR for Eu^{3+} and Yb^{3+} doped silver-containing glass respectively[14,15]. Indeed, the high fluorescent silver cluster strongly absorbing UV and blue light promotes the emission of Eu^{3+} and Yb^{3+} by resonant energy transfer phenomena. However, the f-f transition of rare earth results in a narrow emission bandwidth since the 4f levels are internal orbitals. Wider emission spectra has been reported with metal-alloy element of the periodic table such as Bismuth (Bi) since the discovery of the NIR emission of the low valence Bismuth ions in silica-based glasses[16]. Indeed, the NIR emission of Bi^+ ion exhibits a broad bandwidth covering the second optical communication window[17–20]. Such broad emission band is of particular interest for optical amplifier, for telecommunication and NIR laser applications. Low valence bismuth ion Bi^{2+} is also known as a red luminescent center and can have a great interest in high-power composite LEDs application[17,21–25]. It should be noticed that the stabilization of the different low valence state of bismuth ions highly depend on the nature of the host matrix as well its acidity and basicity[17,26,27]. However, photo-activated low valence bismuth ions can be generated using fs laser or other high ionizing sources[28–34]. In this article, we report highly localized 3D architecture in bismuth doped silver-containing glass induced by fs DLW. This was done by combining laser-induced photochemistry of silver ions for the formation of Ag_m^{x+} and the photo-induced redox reaction to reach low valence Bismuth ions. High localized optical contrast and tuneable luminescence property have been achived leading to a broad emission band from Ag_m^{x+} and Bi^{2+} emitting centers covering the whole visible range, as well as a broad emission band in the NIR from Bi^+ emitting centers. Furthermore, the mechanisms of energy transfer between silver clusters and rare earths[11–15,35,36], as well as between bismuth ions and rare

earths[37–39] were repoted in the litterarture.However from our knowledge, the energy transfer between silver clusters and bismuth ions was not reported before. Thus, we also highlight in this article, the energy transfer phenomena occuring between silver clusters and bismuth ions. The reported results have been repeated with several glass batchs and for various laser irradation series, which ensures the reliaibility and repetability of the present work.

2. Methods

2.1 Glass synthesis and characterization

Bismuth-doped silver-containing phosphate glass samples were synthetized using the following compositional system (100-x)[55$PO_{5/2}$-38ZnO-1$GaO_{3/2}$-5.5$AgO_{1/2}$] − x$BiO_{3/2}$ (atm. %), x equal to 0, 0.17, and 0.33. The theoretical compositions of glasses are shown in the table1. The raw material used to perform this synthesis are H_3PO_4 (Roth, 85%), Na_2CO_3 (Alfa Aesar, 99.95%), Ga_2O_3 (Strem Chemicals, 99.998%), and $AgNO_3$ (Alfa Aesar, 99.995%) and Bi_2O_3 (Sigma-Aldrich, 99.9%). The precursors were homogeneously mixed with an aqueous solution and dried on the sand bath for 12 hours to obtain a cement. The cement was ground and melted at 1050 °C in a platinum crucible for 10 hours. The melt was quenched at room temperature to obtain the final glass samples. The synthesized glass was annealed at 40°C below the T_g for 4 hours to reduce mechanical strength created upon the quenching. A 1 mm thick slice of the glass was optically polished. Table 1 presents the label and the theoretical composition of the studied samples.

Table 1 : Sample compositions

Glass samples	ZnO	$PO_{5/2}$	$GaO_{3/2}$	$AgO_{1/2}$	$BiO_{3/2}$
PZn:Ag	38	55	1.4	5.5	
PZn:Ag0.17Bi	37.87	55.08	1.38	5.5	0.17
PZn:Ag0.33Bi	37.80	55	1.37	5.5	0.33
PZn0.17Bi	38.35	56	5.5		0.17

Cary 5000 spectrophotometer was used to perform the UV-Visible transmission spectra on the pristine glass in the range of 250-1500 nm. Room temperature excitation and emission spectroscopies were performed with a SPEX Jobin Yvon fluorescence spectrometer equipped with a double monochromator, a UV grating blazed at 350 and Peltier cooled PMT (Horiba Jobin Yvon Gmbh, Haching, Germany) for the UV spectrum range. A Xenon lamp was used as the excitation source. This enabled a continuous excitation from 200 to 800 nm and the collected spectra data were corrected from both the spectral lamps distribution, the grating response and the detector sensitivity.

2.2 Femtosecond laser inscription

The 3D modification of the glass where performed using a Ytterbium femtosecond (fs) oscillator (up to 2.6 W, 9.1 MHz, and 390 fs FWHM at 1030 nm). The setup is combined with an acousto-optic modulator, allowing focusing both the energy and the irradiance up to 100 nJ and 20 $TW.cm^{-2}$, respectively. The following irradiances were considered: 3.70, 4.33, 4.79, 5.22 and 5.74 $TW.cm^{-2}$, associated to pulse energies of 3.70, 4.33, 4.79, 5.22 and 5.74 nJ, and corresponding applied energy densities of 3.70, 4.33, 4.79, 5.22 and 5.74 $J.cm^{-3}$. The displacement of the sample during DLW irradiation was performed with a high-precision XMS-50 translation stage (up to 50 nm). The considered sample velocities were 10 $\mu m.s^{-1}$, and from 10 $\mu m.s^{-1}$ to 100 $\mu m.s^{-1}$ in supplementary information, typically corresponding to cumulative laser pulse overlaps from 1.48×10^5 to 1.48×10^6 pulses, respectively. Zeiss microscope objective (40×, 0.75NA) was used to generate the DLW structure at 160 µm below the sample surface. A spatial light modulator (LCOS; X10468-03, Hamamatsu Photonics) was used to eliminate spherical aberrations. The glass sample was moved by means of a three-coordinate motorized magnetic-levitation translation stage (Newport) synchronized with the laser.

2.3 Fluorescence micro-spectroscopy and the hyper-spectral micro-imaging of the structured sample

A high spectral resolution micro-spectrometer (LabRAM HR800 from (Horiba Jobin Yvon GmbH, Haching, Germany) with 1200 $grooves.cm^{-1}$ (for visible) and 300 $grooves.cm^{-1}$ (for NIR) grating using a Peltier cooled CCD camera and liquid nitrogen-cooled InGaAs detector respectively was used to record the fluorescence spectra of the DLW structures. The 405 nm and 532 nm excitations were performed with a OBIS laser (100 mW, TEM_{00}, Coherent, Santa Clara, CA, USA) and a Sapphire SF laser (100 mW, TEM_{00}, mono-mode, Coherent, Santa Clara, CA, USA), respectively. For the excitation and epi-collections an Olympus microscope objective of 50×, 0.9 NA is used. The fluorescence spectra were collected over the range of 425 - 1100 nm and from 900 - 1450 nm.

We performed the Confocal fluorescence imaging with a Leica DM6 CFS TCS SP8 confocal microscope equipped with a 405 nm and 638 nm laser diode, and an immersion microscope objective (Leica, 63×, 1.3NA, index matching oil at n = 1.512).

The fluorescence hyper-spectral micro-imaging was performed using a Picoquant MT200 microscope equipped with a spectrometer and a CCD camera of the full emission spectrum over the visible range up to the NIR detection limit of the detector. The 473 nm excitation is performed with a continuous wave laser diode. The visible and NIR micro-images of the laser-inscribed patterns resulted from the spectral integrations over the 500-700 nm and 920-1050 nm spectral ranges, respectively.

We performed fluorescence lifetime imaging microscopy (FLIM) using a Picoquant MT200 microscope equipped with two MPD single photon avalanche diodes (SPADs) and a PicoHarp300 timing board for

time-correlated single photon counting (TCSPC) operation. A pulsed laser at 375 nm, with pulse duration of 90 ps and a repetition rate of 5 MHz via an acousto-optic pulse picker was used for excitation. A 100 × 1.40NA oil objective (UPLSAPO100XO, Olympus, Tokyo, Japan) was used for both excitation and collection of the fluorescence mounted with a band-pass filter with a transmitted spectral window 425–450 nm. The laser was scanned by means of a piezoelectric stage in a grid pattern of 156 nm steps and 0.6 ms/pixel. For the FLIM images calculation, "FAST-FLIM" algorithm was used and the lifetime distribution was calculation used the method reported by Petit *et al.,*[14].

3. Results and Discussion

3.1 Absorption, excitation and emission spectroscopy of the pristine glass spectroscopy

Absorption spectroscopy covering the UV/Visible/NIR spectrum range, for different cationic concentrations of Bismuth (0 to 0.33%) in silver-containing PZn glasses has been performed and Figure 1.a displays the corresponding linear absorption coefficient of these glasses. It is seen that all the glass exhibits a strong absorption tail in the UV range. For the bismuth-free glass (PZn:Ag), the UV tail is attributed to the strong absorption of silver ions[40]. In the presence of bismuth (PZn:Ag0.17Bi glass), a noticiable redshift of the UV tail is observed, which increases with the increase of bismuth content up to 0.33 atomic percent. Indeed, this redshift is propbably associates to the presence of Bi^{3+} [21]. Further linear absorption spectrum of PZn0.17Bi glass as shown in the the green curve of the Figure 1.a, exhibiting similar UV absorption tail as PZn:Ag0.17Bi glass evidence the occurrence of Bi^{3+} ions transitions in the UV range. Above 300 nm, no significant absorption related to silver clustering or plasmonic effect is observed in silver-containing glasses. In the mean time, in bismuth-doped glasses, we didn't observed any significant absorption from low valence bismuth ions which are typically seen in the visible and the NIR range[28,41,42]. Consequently, silver ions and Bismuth ions are well dispersed in their respective oxidation state Ag^{+} and Bi^{3+}.

Moreover, excitation and emission spectra of silver ions have been conducted on Bismuth-doped PZn:Ag glasses compared to undoped PZn:Ag glass. Figure 1.b evidence the occurrence of isolated Ag^{+} ions excitation band[6,9] for 270 nm emission in the presence of Bi^{3+}. Likewise, for the 370 nm emission the characteristic excitation band of the paired Ag^{+}- Ag^{+} ions occurred (as shown in Figure 1.c)[6,9]. However, a significant feature associated to the shape of the excitation band of the silver ions is observed in the presence of bismuth. This feature could arise from a competitive absorption associate to Bi^{3+}, as Bi^{3+} ions also experience a strong excitation in this spectral range[43] (see Figure#S1 of the supplementary information). For 230 nm excitation, Figure 1.d reveals the characteristic emission bands of Ag^{+} and Ag^{+}- Ag^{+} with their respective spectrum maximum located at 270 nm and 370 nm[6,9]. The relative decrease of Ag^{+} contribution compared to the pair Ag^{+}-Ag^{+} is observed, supporting the competitive absorption phenomenon due to Bi^{3+}. Moreover, the Ag^{+}- Ag^{+} emission band experiences a slight redshift

with bismuth content, which can be associated to contribution of Bi^{3+} emission. When extending the emission spectrum to the red and NIR region (not presented here), no significant emission related to silver clusters, nor low-valence bismuth ions were detected. This imply that only monovalent silver ions (Ag^+ and Ag^+-Ag^+) and trivalent Bi^{3+} ions co-existed in the PZn glass.

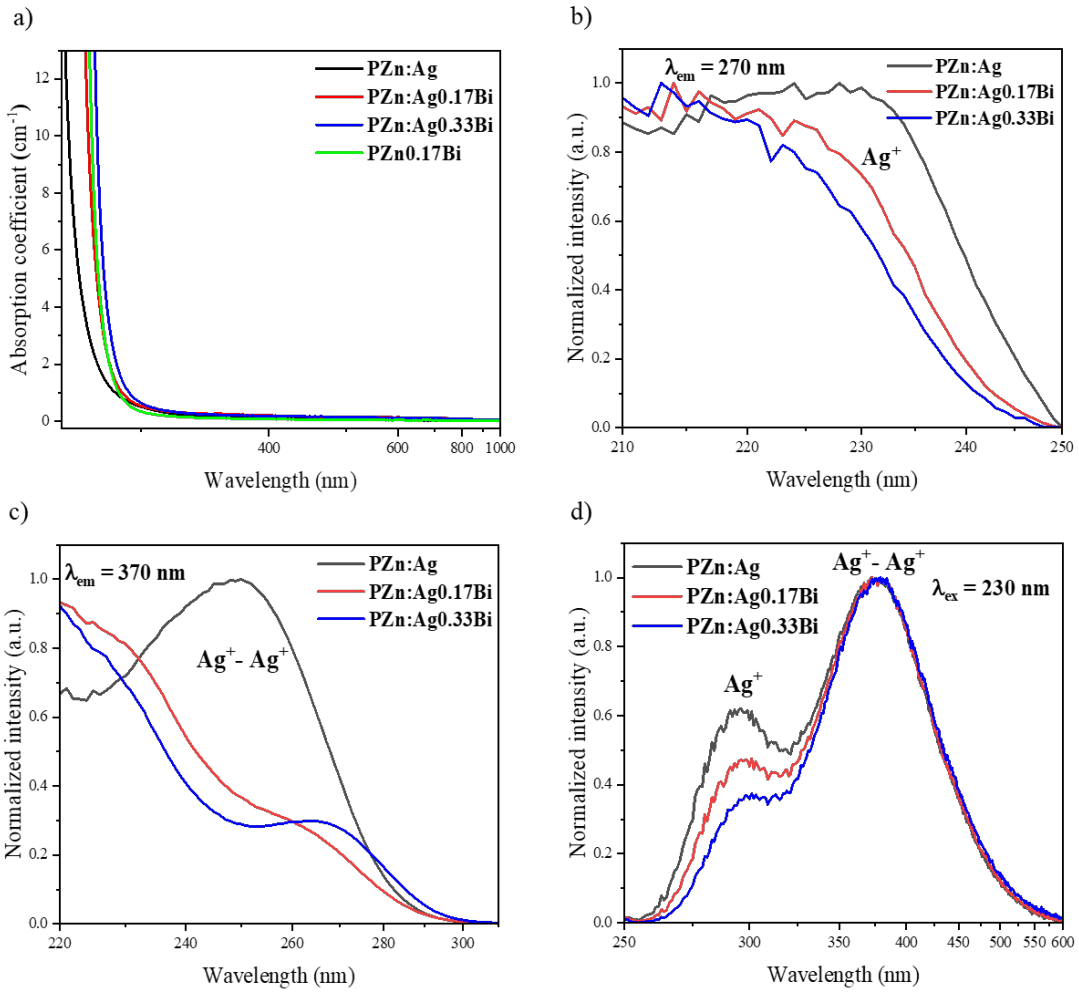

Figure 1. Luminescence properties of the pristine Bismuth-doped silver-containing PZn glasses. (a) Linear absorption coefficients of bismuth-doped silver-containing and silver-free glasses, (b) Excitation spectra of Ag^+ for 270 nm emission, (c) Excitation spectra of Ag^+-Ag^+ for 370 nm emission (d) Emission spectra of Ag^+ and Ag^+-Ag^+ for 230 nm excitation.

3.2 Micro-fluorescence spectroscopy of laser-inscribed patterns

Fs DLW have been performed in PZn:Ag0.17Bi glass, inducing identical square patterns of 50 µm X 50 µm snake like structures resulting from successive laser track of 10 µm interline. Such structures were induced under 160 µm of the glass surface with fixed linear translation of the glass sample of 10 $\mu m.s^{-1}$ speed and different laser irradiances from 3.70 $TW.cm^{-2}$ to 5.74 $TW.cm^{-2}$. Figure 2.a displays the wide field confocal fluorescent image of the laser induce structural patters. In the case of Figure 2.a(i), the experiment was performed with 405 nm excitation and the fluorescence was collected over the range of [480 - 580 nm]. The observed green fluorescence of the pattern is attributed to the molecular silver clusters $(Ag_m^{x+})^9$, formed by a mobile silver atoms Ag^0 and silver ions Ag^+. No fluorescence is seen for

3.70 TW.cm^{-2} laser irradiance. The fluorescence intensity associated to the formation of Ag_m^{x+} increase from 4.33 TW.cm^{-2} up to 5.74 TW.cm^{-2}. However, the Figure 2.a(ii) show the confocal image of the same patterns excited at 638 nm and fluorescence collected over [680 - 750 nm]. The red fluorescence of the patterns cannot be attributed to Ag_m^{x+} as 638 nm is far from the excitation band of Ag_m^{x+}[14,44], and as reported in Figure 2.a(i), no fluorescence of Ag_m^{x+} is observed for the 3.70 TW.cm^{-2} induced pattern. Hence, the red fluorescence of the patterns is probably associated with bismuth ions especially Bi^{2+} which is knew to present a strong fluorescence in this spectral range[17,21,24]. This fluorescence of Bi^{2+} can be seen for 3.70 TW.cm^{-2} where no Ag_m^{x+} fluorescence is detected, suggesting that the presence of bismuth might play a role in the mitigation of Ag_m^{x+} fluorescence at such laser irradiance. To elucidate this, DLW structural matrix with identical laser parameters was induced in both PZn:Ag and PZn:Ag0.17Bi glasses as shown in the Figure#S2 of the supplementary information. As a result, the overall fluorescence intensity of Ag_m^{x+} of the patterns is reduced in the presence of bismuth. This confirms the impact of bismuth ions in the creation of Ag_m^{x+} and its fluorescence efficiency upon fs DLW. Indeed, the formation of Ag_m^{x+} is highly dependent on the Ag^0 which is originated from an electron trapped by Ag^+ ions. With the presence of bismuth, a competitive reaction involving electron transfer between Ag^+ and and Bi^{3+} occurs, during which the reduction of Bi^{3+} with an electron to Bi^{2+} would be more favorable than the electrons capture of silver ions to formed Ag^0. As a consequence the kinetic of Ag_m^{x+} formation will be reduced in the presence of bismuth. This results reveals the inversion of standard redox reaction that may occur based on the gamma rule in aqueous solution where the redox potential of Ag^0/Ag^+ is higher than that of Bi^{3+}/Bi^{2+} as well as Bi^{2+}/Bi^+ couple[45], thus the reduction of Ag^+ to Ag^0 should dominate. On the other hand we can assumed that the activation energy necessary for the formation of fluorescent Ag_m^{x+} under DLW might be affected by the reduction of Bi^{3+}.

The inset of the Figure 2.a shows the magnified image of a given pattern, highlighting double-track fluorescence for both Ag_m^{x+} and Bi^{2+} that might preferentially formed at the edge of the voxel of laser/matter interaction upon the laser passes[15]. These results demonstrated that the interaction of fs laser with PZn:Ag0.17Bi glass trigger both the photochemistry of silver ions and the photo-reduction of Bi^{3+}. Indeed the electron density generated upon the first laser pulses will be simultanouesly involved in the photochemistry and phoredox reactions. This unique feature allows for creating multiscale architectures exhibiting sub-micron features and fluorescence propreties in the green and red range, as shown in Figures 2.a(iii&iv), possibly leading for high-resolution optical standarts for confocal fluorescence optical microscopy calibration in the Vis/NIR, similar to that reported in the case of Ag_m^{x+}/Yb^{3+} [15].

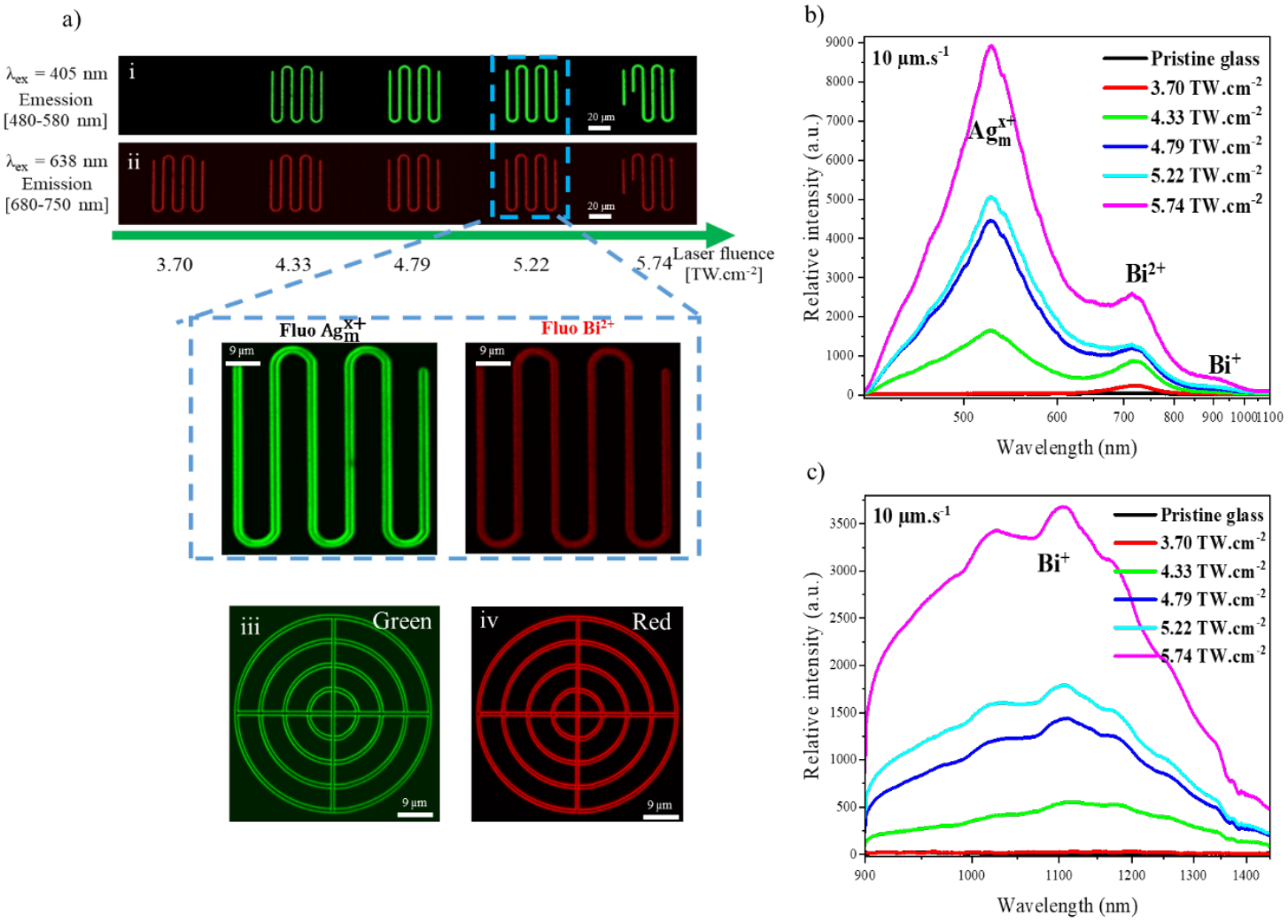

Figure 2. (a) Confocal fluorescence images of laser-inscribed patterns at 10 µm/s for various intensities : (i) 405 nm excitation and fluorescence collection in the 480-580 nm range, (ii) excitation at 638 nm and fluorescence collection in the 680-750 nm range. (iii and iv) Illustration of multi-scale architectures of fluorescent optical standard for confocal microscopy calibration with (iii) green and (iv) red emissions, respectively. (b) Confocal micro-emission spectra of laser-inscribed patterns under 405 nm excitation showing visible and NIR emissions of Ag_m^{x+}, Bi^{2+} and Bi^{+} species. (c) Confocal micro-emission spectra recorded with a nitrogen cooled InGaAs camera showing the Bi^{+} emission in the 900-1400 nm range.

Confocal micro-emission spectroscopy have been performed on the structural patterns of the Figure 2.a. The emission spectra for 405 nm excitation is displayed in Figure 2.b, showing broad band spanning from the visible to the NIR range featuring two main contributions at 525 nm corresponding to Ag_m^{x+} emission[9,14,46] and at 720 nm corresponding to Bi^{2+} emission[17,21,24]. Additional shoulder around 900 nm can be observed. The intensity of the emission bands increases with the increase of the laser irradiance from 4.33 TW.cm^{-2} to 5.74 TW.cm^{-2}. Below 4.33 TW.cm^{-2} at the same 10 µm.s^{-1} velocity, the contribution of Ag_m^{x+} and the NIR's shoulder are not seen, only Bi^{2+} contribution can be observed, supporting the feature shown in the confocal fluorescence image of the Figure 2.a. Notably, when excitated the pristine glass at 405 nm no Ag_m^{x+}, nor Bi^{2+}, nor NIR emission is observed, highlighting that

the visible to NIR emission is only promoted in the laser structured areas co-located with the fluorescence properties. One should notice that the recorded spectra are not corrected by any instrumental responce. Moreever, the shoulder at around 900 nm is associated with an emission in the NIR , not recorded by the CCD camera and the grating used. Using a nitrogen cooled InGaAs detector and an adapted grating, the NIR emission was well resolved starting from 900 nm to 1450 nm with an FWHM around 350 nm as shown in Figure 2.c. The oxcillation displayed by this spectra originate from the spectral filter used for filtering the emission signal. The broadening of this NIR emission can be attributed to the characteristic emission of Bi^{+} ions[17–19,43] as well the contribution of bismuth clusters cations which formed during the laser writing[47,48]. This bismuth clusters may formed by aggregation of Bi^{+} ions and/or with reduced Bi^{0} atoms. As this emission as well as Ag_m^{x+} emission are not seen together for the patterns written with 3.70 $TW.cm^{-2}$ irradiance, it is possible to suggest a strong correlation existing between Ag_m^{x+} and Bi^{+}.

3.3 Co-localization of laser-induced species

The spatial distribution of the laser induces fluorescent centers have been investigated. Figure 3.a displays the hyperspectral fluorescence images of four successive laser passes from the pattern in the inset of the Figure 2.a. The pattern was excited with 473 nm laser diode and the fluorescence images were recorded in various spectral range to distinguish the contribution of the different luminescence centers. Indeed, from the top to the bottom, the first image with green fluorescence is recorded over the 500-580 nm spectral range attributed to Ag_m^{x+} fluorescence. The second image with red fluorescence is recorded in the 650-750 nm spectral range corresponding to the fluorescence of Bi^{2+} ions. However, the third image recorded over the 850-950 nm spectral range, with less fluorescence intensity resulting from Bi^{+}. The red fluorescence color of this image represents a false color by shifting the spectral information of the NIR to match the red region. The result reveals a double track fluorescence for all three fluorescence species: Ag_m^{x+}, $Bi^{2+,}$ and Bi^{+}, which are located in the same laser structured area. By normalizing, the transversal fluorescence profile for these tree fluorescence species as shown in Figure 3.b, each Bi^{2+} fluorescence double-track is more thicker with an internal distance between track closer to the center voxel of the laser/matter interaction. However, Ag_m^{x+} and Bi^{+} fluorescence double-track are sharper and further away from the center of the voxel of the laser/matter interaction. Thus, such double-track modifications could be due to the occurrence of the photo-dissociation and photo-diffusion effect for both silver clusters and Bi^{2+}, similar to that observed in the glasses containing only silver[8,9]. The lower size and high mobility of silver species (Ag^{0} and Ag^{+}) compared to Bismuth ions could explain the higher internal distance of Ag_m^{x+} fluorescence. We can also suggest the higher photo-destruction of created silver clusters in the center of the voxel of the laser/matter interaction compared to Bi^{2+}. In the case of Bi^{+} double-track the photo-diffusion and photo-dissociation phenomena cannot be used to explain the higher internal distance between the double fluorescence tracks, since the size of Bi^{+} ion is

expected to be higher than the size of Bi^{2+} ion. On the other hand, as described above, the fluorescence of Bi^{+} appears only with Ag_m^{x+} fluorescence, suggesting a strong interaction related to energy transfer phenomena between the Ag_m^{x+} and Bi^{+}.

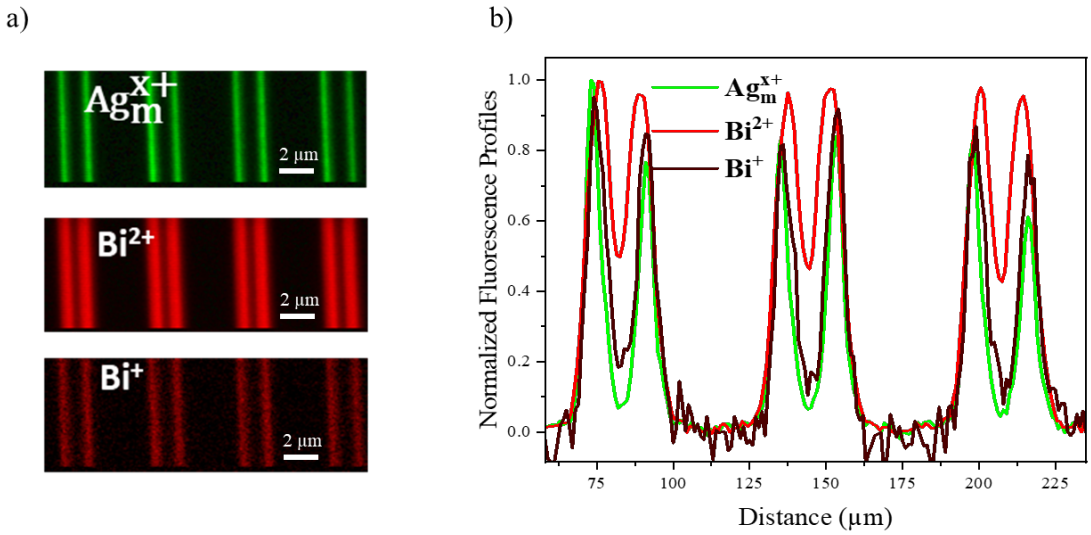

Figure 3. (a) Hyperspectral fluorescence images of the double-track patterns induced with 5.22 $TW.cm^{-2}$ and 10 $\mu m.s^{-1}$ under excitation at 473 nm, showing the spatial distribution of the fluorescence of Ag_m^{x+} (500-580 nm range), Bi^{2+}(650-750 nm range), and Bi^{+} (850-950 nm range). (b) Normalized transverse fluorescence profile for Ag_m^{x+}, Bi^{2+}, and Bi^{+} species.

3.4 Competitive mechanisms of Bi and Ag species formation

Figures 4.a and 4.b present the confocal fluorescent images of the pattern inscribed with the same laser parameter (4.97 $TW.cm^{-2}$ and 10 $\mu m.s^{-1}$) exhibiting Bi^{2+} fluorescence in PZnAg:0.17Bi and PZn0.17Bi glasses, respectively. Notably, the intensity of Bi^{2+} fluorescence in the presence of silver is stronger and exhibits a double-track laser modification. Moreover, without the presence of silver ions, only single-track laser modification is observed at the considered irradiation condition, being associated to a much weaker Bi^{2+} fluorescence emission intensity. Under fs laser irradiation, Ag^{+} ions can get ionized, behaving thus a reservoir to create free electrons[8,10]. Thus, without the presence of silver ions, laser irradiation leads to a much weaker generation of free electrons, leading thus to a much weaker probability to reduce Bi^{3+} ions into Bi^{2+}. The fact that the Bi^{2+} emission shows either a bright double-track feature or a less intense single-track when considering glasses with or without silver, respectively, results from the cumulative multi-pulse management of the silver reservoir[8,10]. In presence of silver, the dynamics of Bi^{2+} creation is dominated by the creation dynamics of free electrons, which is directly linked to the diffusion of silver species from the center of the laser irradiation voxel to its edges, leading to the bright double-track feature. In absence of silver, the free electron dynamics is much less efficient, as it has to come from the glass matrix itself, so that it remains localized at the center of the laser irradiation voxel, leading to the less intense single-track feature. Thus, the significant contrast between Figures 4.a and 4.b corroborates the central role played by silver ions in the reduction reaction of Bi^{3+}

favoring the formation of Bi^{2+} ions. As abovementioned, the bismuth in silver-containing PZn glass could trap electron by preventing the formation of Ag_m^{x+}. This might be due to a rapid reduction of Bi^{3+} with laser-generated electrons from silver ions Ag^+ being ionized in Ag^{2+} ions: this kinetically limits silver ions to trap these electrons to form Ag^0 species and subsequently to participate to the growth of silver clusters. Concerning Bi^+, this species appear after the formation of Bi^{2+} species, and appear to be strictly co-localized with the silver clusters, as evidenced in Figure 3.b. in the considered irradiation conditions. This suggests that such a second reduction step of Bismuth elements results from an electron release directly from the silver clusters during their process of growth and chemical/electrical stabilization. Hence, the Bi^+ species appear to directly follow the spatial distribution of silver clusters Ag_m^{x+}. While fs laser irradiation lead to the full cascade of mechanisms (species diffusion and modification of species reservoirs, successive redox processes and chemical bond formation), it is worth noting that electron-beam irradiation leads to much low free electron creation (several orders of magnitude below what obtained with fs lasers). As a consequence, electron-beam irradiation allows for revealing the initial mechanisms at play such glasses.

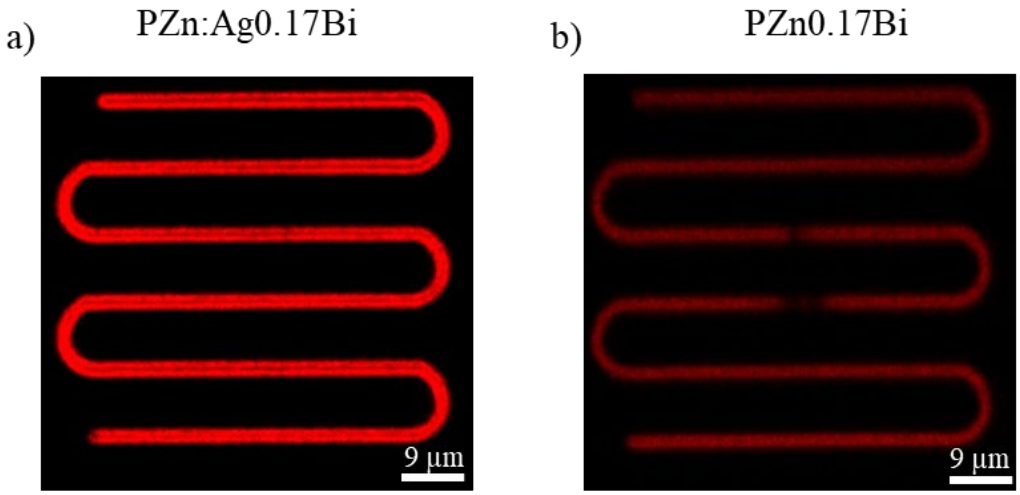

Figure 4: (a,b) Influence of the presence of silver on Bi^{2+} fluorescence in laser-inscribed patterns (4.79 $TW.cm^{-2}$, 10 $\mu m.s^{-1}$) under excitation at 638 nm (collection range : 680-750 nm). Confocal fluorescent images of in PZn:Ag0.17Bi and PZn0.17Bi glasses, respectively.

To elucidate this effect, Electron Spin Resonance (ESR) spectroscopy was conducted on 2.5 MeV electron-irradiated glasses containing silver or bismuth, or both to investigate the process of electron and hole trapping. Indeed, the interaction of the 2.5 MeV electron beam with the glasses will generate a high density of free electrons and holes that could simulate the electron density generated during fs DLW. This allow accessing a high volume of irradiated glass with ESR spectroscopy to access the initial steps involving in the formation of the fluorescence elements. Figure 5.a illustrates the ESR spectra of irradiated PZn:Ag (black curve), PZn:Ag0.17Bi (red-curve), and PZn0.17Bi (blue curve) glasses. For PZn0.17Bi, the ESR spectrum reveals a doublet at 327 mT and 330 mT, corresponding phosphate oxygen hole centers (POHC)[49,50]. No ESR signal that could be attributed to bismuth ions is observed in

this glass. This supports the ongoing debate surrounding the detection of paramagnetic bismuth ions by ESR spectroscopy[51,52]. For the PZn:Ag glass, the ESR signals associated with Ag^0 (302 mT and 362 mT) and Ag^{2+} (280 mT and 318 mT) can be seen[50]. In PZn:Ag0.17Bi glass, the presence of bismuth notably reduced the Ag^0 signals, although the signals of Ag^{2+} experience a slightly reduction in intensity. This result demonstrate that Bi^{3+} can act as trap center for Ag^0, forming low valence bismuth ions Bi^{2+}/Bi^+ as proposed in Figure 5.b, or modifying the stability of Ag^0 in the glass. As consequence, the quantity of Ag^0 diminishes, preventing the formation of silver clusters. Additionally, no signal attributed to silver cluster is observed.

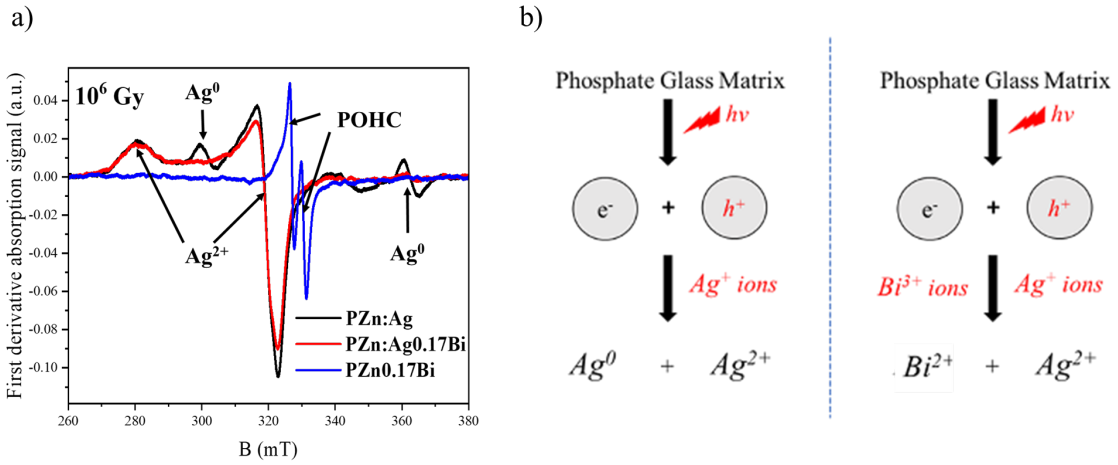

Figure 5: (a) ESR spectrum illustrating the influence of bismuth on silver atom formation under electronic irradiation, showing that Bi^{3+} ions behave as a strong electron scavenger than Ag^+ ions, while hole trap centers remain supported by silver with the formation of Ag^{2+}. (b) Proposed mechanism of electron/hole transfer from the glass matrix to silver ions (left) and to silver and bismuth ions when co-inserted, where electron capture appears more likely to occur from Bi^{3+} ions when existing.

3.5 Energy transfers between silver clusters and Bismuth elements

To investigate the coupling mechanisms between silver species and Bi^{2+} or Bi^+ species on fluorescence emission, we have performed the confocal micro-emission of the patterns of Figure 4. Two excitation sources were used (405 nm and 532 nm), and the emission spectra were collected over the red and NIR range respectively. The 532 nm excitation promotes the emission of both Bi^{2+} and Bi^+ with an enhancement of about 5 times and 10 times, respectively, in presence of silver ions, as shown in the Figure#S4 in the supplementary information. Accordingly, the similar effect was observed for Bi^{2+} emission for the 405 nm excitation (Figure 6.a). At this step, such an enhancement may dominantly result either from an enhanced formation of Bi^{2+} and Bi^+ species in presence of silver and/or from energy transfers from laser-induced silver clusters (these structures being inscribed in each glass with the same laser parameters). However, Figure 6.b reports that the NIR emission of Bi^+ excited at 405 nm shows a quite zero intensity emission (black curve) for a laser-induced structure in the bismuth-containing glass, and a much more intense emission for a laser-induced structure in the bismuth-and-silver-containing glass. This proves that Bi^+ emission is promoted only in presence of Ag_m^{x+} for the same excitation at 405

nm, while there exist Bi^+ species in both the Bismuth-containing and Bismuth-and-silver containing glasses, as proved with Figure#S4 under excitation at 532 nm. As a consequence, the Bi^+ NIR emission under 405 excitation is understood as being fully attributed to energy transfers from laser-induced silver clusters. Therefore, this suggests the ability to activate the NIR emission of Bi^+ indirectly through Ag_m^{x+} by energy transfer phenomena, including for an excitation at 532 nm, much like the phenomena observed in Ag_m^{x+}/Rare earth couples[14,15]. As seen in Figure 3, the fluorescence of Bi^+ tends to be co-localized with that of Ag_m^{x+}, which is highly compatible with non-radiative energy transfer phenomena occurring from Ag_m^{x+} to Bi^+ at short scales (from sub-nm to a few nm). Furthermore, the presence of silver nanoparticle in glass containing bismuth have been reported to enhance the fluorescence emission of Bi^+[53,54]. However, in the present study no plasmonic band from silver nanoparticle was observed: indeed, no surface plasmon resonance from metallic silver NPs and associated absorption band was observed as it is very unlikely to occur at such silver loading in these glasses (without applying a subsequent thermal treatment around the glass transition temperature). Thus, energy transfers appear only where laser irradiation took place, allowing for perfect background-free NIR emission whose excitation is fully mediated by energy transfers, while considering relevant excitation wavelengths.

To gain further insights into the energy transfer mechanism from Ag_m^{x+} to Bi^+, time-resolved spectroscopy of Ag_m^{x+} using FAST-FLIM have been performed. Similar Fs DLW pattern induced in PZn:Ag and PZn:Ag0.17Bi glasses respectively were analyzed. A pulse laser of 90-picosecond and repetition rate of 5 MHz at 375 nm was used for excitation and the fluorescence lifetime was monitored over the spectral range of 400-450 nm to select only the Ag_m^{x+} lifetime. Figure 6.c displays the FAST-FLIM fluorescent lifetime histogram of Ag_m^{x+} extracted from FAST-FLIM images (not shown here) of the patterns. The result shows at typical relative peak value of Ag_m^{x+} mean fluorescence lifetime of 1.21 ns in the presence of bismuth (PZn:Ag0.17Bi), while in the absence of bismuth, the relative peak value of Ag_m^{x+} fluorescence life time is about 2.78 ns. This results an important shortening of Ag_m^{x+} fluorescence lifetime in the presence of bismuth. Moreover, the corresponding exponential decay curve shown in Figure 6.d, which exhibits at least two fluorescence lifetime originating from different Ag_m^{x+} family, experiences a shortening of all fluorescence lifetime with a quenching intensity of about 5.5 times. This result confirms a strong quenching of Ag_m^{x+} fluorescence through the energy transfer mechanism from Ag_m^{x+} to Bi^+ ions with a quenching rate corresponding to $Q_{\tau_{Ag,Bi^+}/\ \tau_{Ag}} = 1 - \ \tau_{Ag,Bi^+}/\ \tau_{Ag}$ about 56%, much higher than the quenching rate observed in the case of Ag_m^{x+} /rare earths couple[14,15]. This showcase a more efficient non-radiative energy transfer phenomenon between Ag_m^{x+} and Bi^+.

The shortening of the emission decay time of the silver clusters in the presence of bismuth and the concomitant enhancement of Bismuth emission suggests the occurrence of a non-radiative energy

transfer. Concerning the mechanism, Dexter and FRET processes can be anticipated. In both cases, the energy transfer is expected to occur at short distances (from contact to a few nm). Indeed, 'Dexter' is an electron exchange mechanism, requiring an overlap of the electronic orbitals of donor and acceptor. Concerning FRET, the strong overlap between the emission spectra of silvers clusters and the excitation spectra of Bi^{+} [20] is allowing the occurrence of such a mechanism. However, the very weak absorption coefficient of bismuth ions in the glass matrix, as well as the short lifetime of the donor, are not favorable for long distance energy transfer. The discrimination between both processes, in any case probably occurring at very short distances, would be difficult experimentally and requires theoretical approaches, which are beyond the scope of the present article.

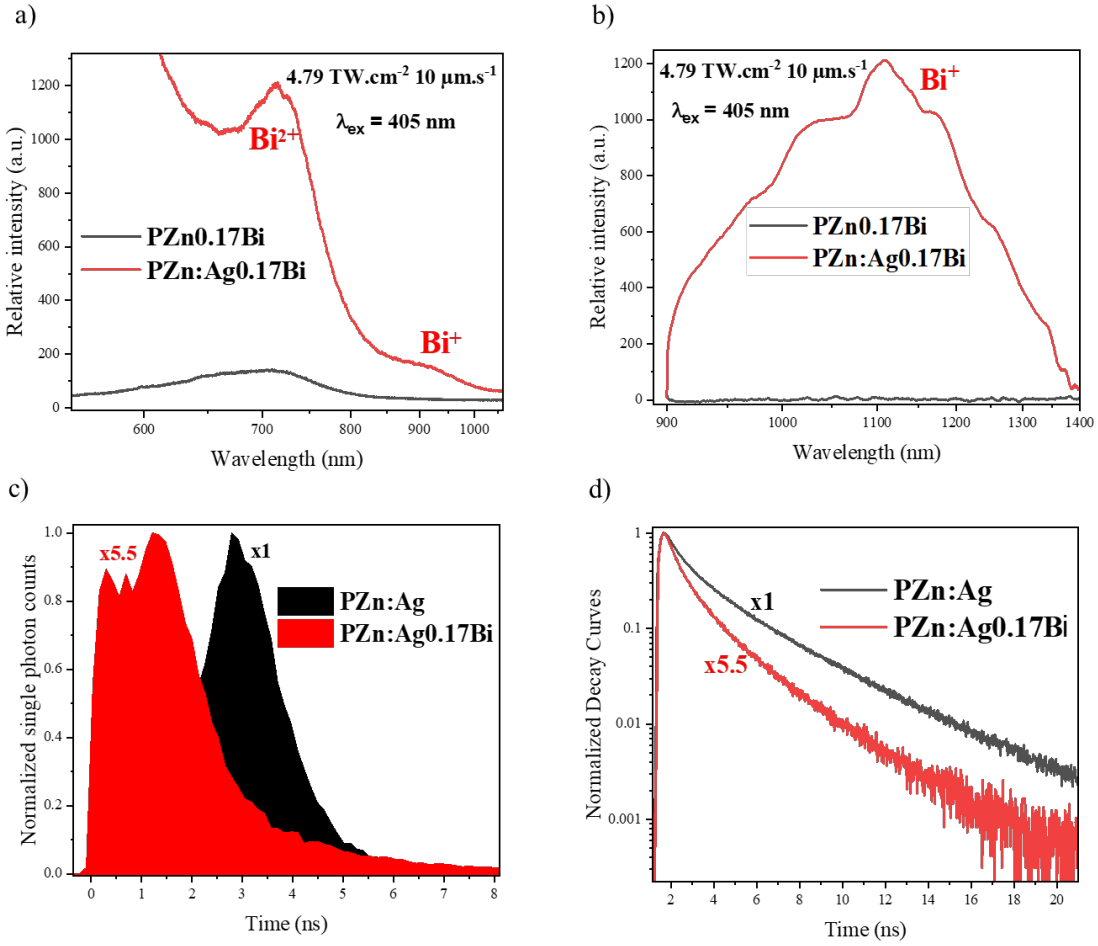

Figure 6. (a,b) Confocal micro-emission spectroscopy of Bi^{+} and Bi^{2+} ions for 405 nm excitation, respectively, of the considered laser-inscribed pattern in both PZn0.17Bi and PZn:Ag0.17Bi glasses. (c) Histogram of time-correlated single-photon fluorescence emission from silver clusters under excitation at 375 nm, in both PZn0.17Bi and PZn:Ag0.17Bi glasses (patterns with 4.79 $TW.cm^{-2}$, 10 $\mu m.s^{-1}$). (d) Associated decay times of Ag_m^{x+} fluorescence showing both their lifetime shortening and amplitude decrease, demonstrating energy transfers from Ag_m^{x+} to Bismuth elements.

4. Conclusion

We have demonstrated that the insertion of Bi^{3+} ions in a silver-containing photosensitive glass preserves the femtosecond laser activation of the photochemistry of silver, which allows for producing highly-

efficient broadband fluorescent silver clusters and associated 3D-localized patterns with sub-micron features. While silver cluster fluorescence covers the blue-green spectral range, the insertion of Bi^{3+} ions allows for remarkably extending the span of the spectral range of the laser-inscribed patterns, by adding red (around 700 nm) and NIR (900-1400 nm) bands. The new emitting bands results from the formation of new species, namely Bi^{2+} and Bi^{+}, respectively. The redox mechanisms for Bi^{2+} and Bi^{+} formation are detailed, correlatively to the formation of silver clusters, which describes the central role of silver ions and silver clusters in the efficient formation of new degrees of oxidation of Bismuth. While silver ions behave as both electron trap and hole trap centers, the insertion of Bi^{3+} ions modifies such a dynamics as Bi^{3+} ions are proved to behave as even more efficient free electron scavenger, as clearly evidenced by electron-beam irradiation and subsequent ESR spectroscopy. The formation of Bi^{2+} tends thus to limit the formation of silver clusters in the early stages of this process under femtosecond laser irradiation, while Bi^{+} ions appear to get stabilized and created at the strictly co-localization of silver clusters.

Furthermore, as far as we know, we have demonstrated in the present article the first efficient non-radiative energy transfer from Ag_m^{x+} to a metal transition ion Bi^{+}. Indeed, energy transfer is clearly evidenced by a lifetime shortening of the silver clusters under FLIM microscopy, from 2.78 ns down to 1.21 ns which corresponds to a quenching rate of 56%. Such energy transfers appear even more efficient than those recently observed with rare earth ions. These evidences allow for producing a remarkable background-free 3D-localized NIR emitting patterns while the emitters are being locally produced under femtosecond laser irradiation. Such patterns open new perspectives in terms of designing new pairs of acceptors and donors bearing efficient energy transfers to achieve highly-localized emission in new spectral ranges, which can be of high interest for producing high-quality optical standards for the calibration of the future generation of IR confocal microscopes.

Supporting Information: Excitation and Emission spectroscopy of Bi^{3+}; wide field fluorescence images of DLW induced pattern with different laser intensity and sample displacement velocity in PZn:Ag glass and PZn:Ag0.17Bi glass; wide field confocal fluorescence images of laser inscribed patterns for 405 nm excitation and fluorescence in 480 nm - 580 nm range, excitation at 638nm and fluorescence in 680 nm -750 nm range; emission spectrum of Bi^{+} ions and Bi^{2+} ions respectively of a DLW pattern in both PZn0.17Bi and PZn:Ag0.17Bi glasses for 532 nm excitation.

Acknowledgment: This research has benefited from financial support from French National Research Agency (ANR) ANR-19-CE08-0021-01, and from Région Nouvelle Aquitaine (project AAPR2020-2019-8193110). We acknowledge the financial support from the Grand Research Program « LIGHT » Idex University of Bordeaux, and the Graduate program « EUR Light S&T » PIA3 ANR-17-EURE-0027.

References

1. Davis, K. M., Miura, K., Sugimoto, N. & Hirao, K., Writing waveguides in glass with a femtosecond laser. *Opt. Lett.* **21**, 1729 (1996).
2. Gross, S. & Withford, M. J. Ultrafast-laser-inscribed 3D integrated photonics: Challenges and emerging applications. *Nanophotonics* **4**, 332–352 (2015).
3. Sugioka, K., Cheng, Y. & Midorikawa, K., Three-dimensional micromachining of glass using femtosecond laser for lab-on-a-chip device manufacture. *Appl. Phys. A Mater. Sci. Process.* **81**, 1–10 (2005).
4. Osellame, R., Hoekstra, H. J. W. M., Cerullo, G. & Pollnau, M., Femtosecond laser microstructuring: An enabling tool for optofluidic lab-on-chips. *Laser Photonics Rev.* **5**, 442–463 (2011).
5. Richardson, D. J. Filling the light pipe. *Science* **330**, 327–328 (2010).
6. Royon, A., Bourhis, K., Bellec, M., Papon, P., Bousquet, B., Deshayes, Y., Cardinal, T., and Canioni, L., Silver clusters embedded in glass as a perennial high capacity optical recording medium. *Adv. Mater.* **22**, 5282–5286 (2010).
7. Bourhis, K., Royon, A., Papon, G., Bellec, M., Petit, Y., Canioni, L., Dussauze, M., Rodriguez, V., Binet, L., Caurant, D., Formation and thermo-assisted stabilization of luminescent silver clusters in photosensitive glasses. *Mater. Res. Bull.* **48**, 1637–1644 (2013).
8. Guérineau, T., Fargues, A., Lapointe, J., Vallée, R., Messaddeq, Y., Canioni, L., Petit, Y., and Cardinal, T., Laser Direct Writing of Silver Clusters-Based Subwavelength Periodic Structures Embedded in Mid-Infrared Gallo-Germanate Glass. *Adv. Photonics Res.* **3**, 2200032 (2022).
9. Petit, Y., S., Guérineau, T., Khalil, A. A., Le Camus, A., Fargin, E., Duchateau, G., Bérubé, J-P., Vallée, R., Messaddeq, Y., Cardinal, T. et al, On the femtosecond laser-induced photochemistry in silver-containing oxide glasses: Mechanisms, related optical and physico-chemical properties, and technological applications. *Advanced Optical Technologies* vol. 7 291–309 (2018).
10. Smetanina, E., Chimier, B., Petit, Y., Varkentina, N., Fargin, E., Hirsch, L., Cardinal, T., Canioni, L., and Duchateau, G., Modeling of cluster organization in metal-doped oxide glasses irradiated by a train of femtosecond laser pulses. *Phys. Rev. A* **93**, 013846 (2016).
11. Ma, R., Qian, J., Cui, S., Qiao, X., Wang, F., Fan, X., Enhancing NIR emission of Yb^{3+} by silver nanoclusters in oxyfluoride glass. *J. Lumin.* **152**, 222–225 (2014).
12. Shi, Y., Ye, S., Yu, J., Liao, H., Liu, J., Wang, D., Simultaneous energy transfer from molecular-like silver nanoclusters to Sm^{3+}/Ln^{3+} (Ln = Eu or Tb) in glass under UV excitation. *Opt. Express* **27**, 38159-38167 (2019).
13. Malta, O. L., Santa-Cruz, P. A., De Sá, G. F. & Auzel, F., Fluorescence enhancement induced by the presence of small silver particles in Eu^{3+} doped materials. *J. Lumin.* **33**, 261–272 (1985).
14. Petit, Y., Galleani, G., Raffy, G., Desmoulin, J-C., Jubera, V., Del Guerzo, A., de Camargo A.S.S., Canioni, L., and Cardinal, T., Three-dimensional high spatial localization of efficient resonant energy transfer from laser-assisted precipitated silver clusters to trivalent europium ions. *Crystals* **11**, 148 (2021).
15. Alassani, F., Galleani, G., Raffy, G., Del Guerzo, A., Royon, A., Bourhis, K., de Camargo, A.S.S., Jubera, V., Canioni, L., Cardinal, T. et al, (INVITED) Direct laser writing of visible and near infrared 3D luminescence patterns in glass. *Opt. Mater. X* **16**, 100205 (2022).
16. Fujimoto, Y. & Nakatsuka, M., Infrared luminescence from bismuth-doped silica glass. *Japanese J. Appl. Physics, Part 2 Lett.* **40**, 279-281 (2001).
17. Ren, J., Qiu, J., Chena, D., Hua, X., Jiang, X., Zhua, C., Luminescence properties of bismuth-doped lime silicate glasses. *J. Alloys Compd.* **463**, 5-8 (2008).
18. Yu, P., Su, L., Guo, W. & Xu, J., Broadband infrared luminescence in Bi-doped silicate glass. *J. Non. Cryst. Solids* **464**, 34–38 (2017).
19. Meng, X., Qiu, J., Peng, M. & Chen, D., Near infrared broadband emission of bismuth-doped aluminophosphate glass. **13**, 45–50 (2005).
20. Yong, Z. J., Zhou, Y., Liu, B. M., Zhou, D. D. & Sun, H. T., A Soft Chemistry-Based Route to Near-Infrared Luminescent Bismuth-Activated Glass Films. *J. Am. Ceram. Soc.* **100**, 133–140 (2017).

21. Denker, B. I., Galagan, B. I., Shulman, I. L., Sverchkov, S. E. & Dianov, E. M., Bismuth valence states and emission centers in Mg-Al-silicate glass. *Appl. Phys. B Lasers Opt.* **103**, 681–685 (2011).
22. Peng, M. & Wondraczek, L. Bi^{2+}-doped strontium borates for white-light-emitting diodes. *Opt. Lett.* **34**, 2885 (2009).
23. Dan, H. K., Phan, A. L., Ty, N. M., Zhou, D. & Qiu, J., Optical bandgaps and visible/near-infrared emissions of Bi^{n+}-doped (n = 1, 2, and 3) fluoroaluminosilicate glasses via Ag^{+}-K^{+} ions exchange process. *Opt. Mater. (Amst).* **112**, 110762 (2021).
24. Sun, H. T., Zhou, J. & Qiu, J., Recent advances in bismuth activated photonic materials. *Prog. Mater. Sci.* **64**, 1–72 (2014).
25. Srivastava, A. M., Luminescence of divalent bismuth in M^{2+} BPO5 (M^{2+} = Ba^{2+}, Sr^{2+} and Ca^{2+}). *J. Lumin.* **78**, 239–243 (1998).
26. Dan, H. K., Qiu, J., Zhou, D. & Wang, R., Broadband near-infrared emission and energy transfer in Nd-Bi co-doped transparent silicate glass-ceramics for optical amplifiers. *Opt. Mater. (Amst).* **85**, 517–522 (2018).
27. Chi, G., Zhou, D., Song, Z. & Qiu, J., Effect of optical basicity on broadband infrared fluorescence in bismuth-doped alkali metal germanate glasses. *Opt. Mater. (Amst).* **31**, 945–948 (2009).
28. Kononenko, V., Pashinin, V., Galagan, B., Sverchkov, S., Denker, B., Konov, V., and Dianov, E., Activation of color centers in bismuth glass by femtosecond laser radiation. *Laser Phys.* **21**, 1585–1592 (2011).
29. Yang, W., Corbari, C., Kazansky, P. G., Sakaguchi, K. & Carvalho, I. C., Low loss photonic components in high index bismuth borate glass by femtosecond laser direct writing. *Opt. Express* **16**, 16215 (2008).
30. Wang, L., Cao, J., Lu, Y., Li, X., Xu, S., Zhang, Q., Yang, Z., and Peng, M., In situ instant generation of an ultrabroadband near-infrared emission center in bismuth-doped borosilicate glasses via a femtosecond laser. *Photonics Res.* **7**, 300 (2019).
31. Psaila, N. D., Thomson, R.R., Bookey, H.T., Kar, A.K., Chiodo, N., Osellame, R., Cerullo, G., Brown, G., Jha, A., and Shen, S., Femtosecond laser inscription of optical waveguides in bismuth ion doped glass. *Opt. InfoBase Conf. Pap.* **14**, 1515–1517 (2007).
32. Peng, M., Zhao, Q., Qiu, J. & Wondraczek, L., Generation of Emission Centers for Broadband NIR Luminescence in Bismuthate Glass by Femtosecond Laser Irradiation. *J. Am. Ceram. Soc.* **92**, 542–544 (2009).
33. Zhou, S., W., Chen, J., Hao, J., Zeng, H., and Qiu, J., Laser-induced optical property changes inside Bi-doped glass. *IEEE Photonics Technol. Lett.* **21**, 386–388 (2009).
34. Shen, W., Ren, J., Baccaro, S., Cemmi, A. & Chen, G., Broadband infrared luminescence in γ-ray irradiated bismuth borosilicate glasses. *Opt. Lett.* **38**, 516 (2013).
35. Zhao, J., Yang, Z., Yu, C., Qiu, J. & Song, Z., Preparation of ultra-small molecule-like Ag nano-clusters in silicate glass based on ion-exchange process: Energy transfer investigation from molecule-like Ag nano-clusters to Eu^{3+} ions. *Chem. Eng. J.* **341**, 175–186 (2018).
36. Guérineau, T., Fargues, A., Petit, Y., Fargin, E. & Cardinal, T., The influence of potassium substitution for barium on the structure and property of silver-doped germano-gallate glasses. *J. Non. Cryst. Solids* **566**, 120889 (2021).
37. Li, Y., Sharafudeen, K., Dong, G., Ma, Z. & Qiu, J., Investigation of energy transfer mechanisms between Bi^{2+} and Tm^{3+} by time-resolved spectrum. *Spectrochim. Acta - Part A Mol. Biomol. Spectrosc.* **115**, 305–308 (2013).
38. Dan, H. K., Qiu, J., Zhou, D. & Wang, R., Broadband near-infrared emission and energy transfer in Nd-Bi co-doped transparent silicate glass-ceramics for optical amplifiers. *Opt. Mater. (Amst).* **85**, 517–522 (2018).
39. Xue, J., Wang, X., Jeong, J. H. & Yan, X., Spectral and energy transfer in Bi^{3+}-Re^{n+} (n = 2, 3, 4) co-doped phosphors: Extended optical applications. *Phys. Chem. Chem. Phys.* **20**, 11516–11541 (2018).
40. Maurel, C., Cardinal, T., Bellec, M., Canioni, L., Bousquet, B., Treguer, M., Videau, J.J., Choi, J., and Richardson, M., Luminescence properties of silver zinc phosphate glasses following different irradiations. *J. Lumin.* **129**, 1514–1518 (2009).

41. Dianov, E. M., Bismuth-doped optical fibers: a challenging active medium for near-IR lasers and optical amplifiers. *Light Sci. Appl. 2012 15* **1**, e12–e12 (2012).
42. Peng, M., Wang, C., Chen, D., Qiu, J., Jiang, X. and Zhu, C., Investigations on bismuth and aluminum co-doped germanium oxide glasses for ultra-broadband optical amplification. *J. Non. Cryst. Solids* **351**, 2388–2393 (2005).
43. Yan, N., Xiong, P., Liu, B., Song, X., Shi, Z., Xiao, Y., Wu, M., Wei1, B., Tang, G., Tian, S., et al, Z., Heat treatment to regulate bismuth valence toward enhanced radiation resistance in barium gallo-germanate glass. *J. Am. Ceram. Soc.* **106**, 1240–1249 (2023).
44. Marquestaut, N., Petit, Y., Royon, A., Mounaix, P., Cardinal, T., and Canioni, L., Three-Dimensional Silver Nanoparticle Formation Using Femtosecond Laser Irradiation in Phosphate Glasses: Analogy with Photography. *Adv. Funct. Mater.* **24**, 5824–5832 (2014).
45. Singh, S. P. & Karmakar, B. A New Synthesis Approach and Properties of Bismuth Coated Spherical to Hexagonal Silver Nanoparticles in Dichroic Ag : Bismuth Glass Nanocomposites. *Plasmonics* 6, 457–467 (2011).
46. Bourhis, K., Royon, A., Bellec, M., Choi, J., Fargues, A., Treguer, M., Videau, J.J., Talaga, D., Richardson, M., Cardinal, T. et al, Femtosecond laser structuring and optical properties of a silver and zinc phosphate glass. *J. Non. Cryst. Solids* **356**, 2658–2665 (2010).
47. Sun, H. T., Matsushita, Y., Sakka, Y., Shirahata, N., Tanaka, M., Katsuya, Y., Gao, H., and Kobayashi, K., Synchrotron X-ray, photoluminescence, and quantum chemistry studies of bismuth-embedded dehydrated zeolite y. *J. Am. Chem. Soc.* **134**, 2918–2921 (2012).
48. Romanov, A. N., Serykh, A. I., Haula, E. V., Shashkin, D. P., Kogan, V. M., Rozhdestvenskaya, N. N., Krylov, I. B., and Korchak, V. N., NIR photoluminescence of ZSM-5 and mordenite zeolites, containing low-valence bismuth exchange cations. *Microporous Mesoporous Mater.* **336**, 111875 (2022).
49. Griscom, D. L., Friebele, E. J., Long, K. J.and Fleming, J. W., Fundamental defect centers in glass: Electron spin resonance and optical absorption studies of irradiated phosphorus-doped silica glass and optical fibers. *J. Appl. Phys.* **54**, 3743–3762 (1983).
50. Alassani, F., Desmoulin, J-C., Cavani, O., Petit, Y., Cardinal, T., and Ollier, N., Silver Photochemical reactivity under electronic irradiation of Zinc-Phosphate and Sodium Gallo-Phosphate glasses. *J. Non-Cryst. Solids* **600**, 122009 (2023).
51. Peng, M., Qiu, J., Chen, D., Meng, X. & Zhu, C. Superbroadband 1310 nm emission from bismuth and tantalum codoped germanium oxide glasses. *Opt. Lett.* **30**, 2433 (2005).
52. Sun, H.-T., Sakka, Y., Shirahata, N., Matsushita, Y., Deguchi, K., and Shimizu, T., NMR, ESR, and Luminescence Characterization of Bismuth Embedded Zeolites Y. *J. Phys. Chem. C* 117, 6399−6408 (2013).
53. Martins, M. M., Silva, D. S., Kassab, L. R. P., Ribeiro, S. J. L., and De Araújo, C. B., Enhancement of Optical Absorption, Photoluminescence and Raman Transitions in Bi_2O_3-GeO_2 Glasses with Embedded Silver Nanoparticles. *Artic. J. Braz. Chem. Soc* **26**, 2520 (2015).
54. He, X., Xu, X., Shi, Y. & Qiu, J. Effective enhancement of Bi near-infrared luminescence in silicogermanate glasses via silver-sodium ion exchange. *J. Non. Cryst. Solids* **409**, 178–182 (2015).